

A Convolutional Neural Network for Outsole Recognition

Abstract

To assess random match probability at the level of class characteristics, one could imagine sampling shoes from a local population and calculating the proportion of shoes "similar" to a given print. Our proposed implementation of such a procedure involves 1) a scanner to gather images of shoes from a local population and 2) software to automatically label images within a feature space and assess the images for similarity among those features. In this paper, we discuss an algorithm for automatically labeling shoe outsole images using a **classification scheme** similar to what examiners use: a set of features based on geometric shapes such as circles, stars, and quadrilaterals. The automatic labeling algorithm performs well on images with unambiguous shapes and moderate color contrast, though some systematic errors arise from the physical similarities of geometric shapes. Additional improvements may be realized by modifying the labeling scheme to reduce feature overlap and by preprocessing the images to improve contrast. This new approach represents a significant step toward making tractable the computation of random match probabilities of tread patterns, and could potentially be modified to automate other types of footwear examinations based on class characteristics.

Keywords: Footwear; class characteristics; **random match probability**; computer vision; neural networks

1. Introduction

In the United States, forensic analysis of shoe print evidence is varied and difficult. The process of collecting print evidence from a crime scene is not standardized, and it is often impossible to conduct an individualizing analysis (i.e.,

5 one based on randomly acquired characteristics) when a print is partial or of
low quality. In fact, the majority of footwear examinations in the United States
reach conclusions regarding the correspondence of class characteristics rather
than of individualizing characteristics [1]. In the cases where individualizing
characteristics are not used, it may be both possible and useful to assess the
10 random match probability of the footwear evidence at the level of class characteris-
tics; in other words, given a questioned shoe print, what is the probability
that a randomly selected shoe in the relevant population has a similar tread
pattern? Note that this question is distinct from make and model determina-
15 tion since many shoes of different makes and models can still have similar tread
patterns (e.g., knockoffs, similar models over different years, etc). [This is an
important point. Should I make a bigger deal out of it throughout the paper?]

From a statistical perspective, random match probability could theoretically
be calculated by sampling a large number of shoes from a given population and
calculating the observed proportion of shoes in the sample whose tread patterns
20 are similar to the given print. In practice, one potential method of sampling
could be a low-profile scanner placed in a high traffic area. Such a scanner could
take impressions or pictures of shoes walking past, and those scans could then
be used to create a database of shoes relevant to the local area.

A number of footwear studies (such as those by [2] and [3]) have demon-
25 strated that even a couple hundred shoe prints constitute an unwieldy amount
of data, which then require a large amount of time and effort to process and
analyze. Thus, in parallel with the development of the aforementioned scanner,
it is necessary to develop a way to process large amounts of data automatically.
The primary focus of this paper is the development of one such method for
30 large-scale automatic data processing.

Although footwear impressions are more commonly used in practice for
footwear analysis than outsole images, our early prototypes of a footwear scanner
have suggested that cameras are more robust than pressure scanners for
placement in public locations, which may experience inclement weather or other
35 non-controlled conditions. Thus, we are working to develop a scanner that uses



Figure 1: Images of the prototype scanner for collecting a large number of outsole images.

cameras to take pictures of shoe outsoles, much like images that are currently found on the websites of online shoe retailers Figure 1. Despite the fact that images from the scanner would be more degraded in some ways than images found from online retailers, the fundamental requirements to analyze such data would be similar, so retailer images provide a reasonable basis for the development of a method to assess similarity in tread images. More specifically, this assessment is done by identifying a set of relevant features and using image analysis methods to detect the presence or absence of the features in each image, and then defining similarity measures based on those features to determine how many shoes have a tread pattern similar to the pattern of interest.

1.1. Image Analysis

Several attempts have been made to automatically identify features in both prints and shoe tread images, with low-level image analysis methods including fractal decomposition [4], scale-invariant feature recognition [5], Fourier-Mellin transformation [6], and other classical image analysis methods. Some of these low-level methods perform relatively well in good conditions [7] but have degraded performance under conditions which are suboptimal, including those commonly found at crime scenes.

In the wider field of computer vision, attention has turned to more robust

55 methods for image recognition, such as convolutional neural networks (CNNs),
which are capable of achieving near-human accuracy under even degraded image
conditions [8]. These networks are designed to mimic the process of human
vision, and typically involve application of sets of filters, some of which mimic
the filters used in the low-level techniques used in early automatic classification
60 attempts. CNNs have been applied in footwear forensics, making use of more
general neural networks optimized to detect objects found in natural scenes,
such as trees, animals, buildings, and cars; the pre-trained network's features
are then used to compare shoes or prints to determine how well they match [9,
10, 11]. Neural network methods appear to be more successful than traditional
65 image analysis techniques, but the features used for matching are not generally
informative for humans, who typically classify shoes by patterns and spatial
relationships [12, 13].

In this paper, we discuss an alternate approach that uses an additional model
layer to transfer the feature vector output into a vector of probabilities represent-
70 ing the detection of geometric elements in shoe tread images. Working within the
feature space used by forensic examiners allows us to augment human-identified
features with model output, assessing similarity of different shoe images on a
feature set that is explicitly relevant to the domain. **These output probabilities**
can later be used to quantify similarity between tread patterns for the ultimate
75 goal of calculating random match probability for a given tread pattern.

2. Materials and Methods

Images collected from a footwear scanner (as described in the previous sec-
tion) would be stored in photographic form; as a result, we must use image
analysis methods to create numerical features from the original visual record.
80 There are a number of methods that may be employed to identify shapes and
features in an image, such as Fourier-Mellin transforms, Hough transformations
[14] and other low-level feature extraction methods aimed at detecting specific
shapes, such as edges, corners, blobs, or ridges [15, Ch 15]. While these meth-

ods are useful in identifying these specific features at a low level, they only
85 identify features on a very small scale; as a result, they cannot reliably identify
large geometric shapes like those that may be found in a high resolution outsole
image.

Convolutional neural networks (CNNs) are widely recognized as superior for
novel image classification and feature detection. CNNs are a form of artificial
90 neural network which make use of the image convolution operator used by many
low-level feature extraction methods, with the additional ability to aggregate
such features and meaningfully connect them to a pre-determined set of labels.
CNNs have deep architectures that can be trained to identify complex patterns,
but they are structurally similar to the architecture of the human visual system
95 and output binary or probabilistic predictions for given labels that are readily
interpretable. As CNNs make use of labeled training data, the predictions gen-
erated are for features which are similar to those identified by humans, resulting
in models with greater face validity. Once a CNN is trained, it is relatively fast
and easy to apply the model to new images and obtain classifications.

100 *Transfer Learning.* Neural networks are composed of sets of layers; the early
layers, which are called the model base, contain feature detectors, and the final
layers make up the classifier, or model head, which connects meaningful fea-
tures to classification labels (see Figure 2 for an example of the structure of a
105 CNN). Each of these layers is composed of sets of weights and connections that
are optimized during training. A relatively simple convolutional neural network
which processes image data may contain more than 14 million parameters in
the model base and an additional 120 million parameters in the model head;
to train a model of this nature requires millions of labeled images and a sig-
nificant amount of computational power. Assembling sufficient data to train a
110 network from scratch is a gargantuan task; the process of *transfer learning* is a
natural solution to this common problem. Transfer learning leverages the mod-
ularity of neural networks, that is, that the model base that detects features can
be separated from the classifier which produces predictions. Transfer learning

approaches use the base of a model trained on more general image data and
115 train a new model head or classifier using a smaller set of domain-specific labeled images[16]. This allows CNNs to be applied to smaller datasets of several thousand images, reduces the amount of computational time required to fit the model, and provides boosted performance compared to training a new model from scratch [17]. Transfer learning has been successfully applied in automatic
120 classification of medical images [18] as well as in various applications of shoe forensics [10, 9, 11].

Many convolutional neural networks have been trained on a subset of images from an online image database called ImageNet [19]. In particular, there is a standard set of images from ImageNet, consisting of 1.2 million images that span
125 1,000 categories, that is commonly used in computer vision tasks. CNNs trained on ImageNet are optimized for general human-like vision, that is, the ability to recognize a large set of different features simultaneously. As a result, the base of networks trained on these sets are often used for transfer learning, because the initial layers are broadly generalizable to a wide variety of more specific image labeling tasks. In the next section, we will introduce the pre-trained network
130 VGG16, pictured in Figure 2, and examine a selection of its filters (shown in Figure 3) that demonstrate the levels of detail in the initial layers of a model trained on generic data.

VGG16. Developed by Oxford’s Visual Graphics Group, VGG16 is a CNN
135 trained on ImageNet [8]. In contrast to other popular pre-trained networks, such as AlexNet or ResNet, VGG has a relatively simple structure that provides easier training and interpretability with very little sacrificed accuracy. The simplicity of this structure provides the ability to peer into the inner workings of the network for diagnostic purposes, providing a distinct advantage over more
140 complicated network structures with slightly higher accuracy ratings. VGG16 is a common choice for transfer learning because of this structural simplicity; it has been used for detection of text in natural images [20], medical imaging classification [16], classification of weld defects [21], and many other domain-specific

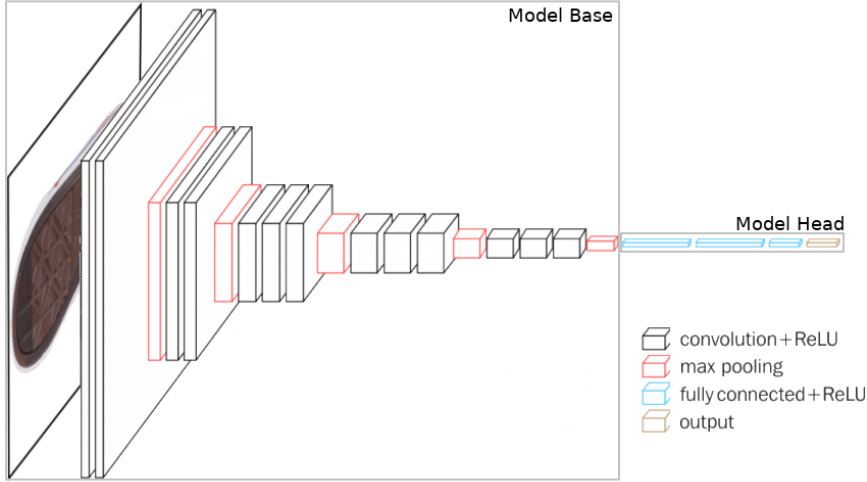


Figure 2: VGG16 consists of five convolutional blocks that make up the model base. Each convolutional block contains an increasing number of increasingly complex feature-detecting filters. After the convolutional blocks, the fully connected layers of the model head are used to make global connections between separate features.

image recognition tasks that are more specific than the ImageNet data on which
 145 it was trained. Figure 2 shows the architecture of VGG16; with transfer learning,
 it is replaced with a model head trained specifically to recognize shoepoint class characteristics.

The base of VGG16 is made up of five convolutional blocks, each of which contain between 128 and 1,536 filters. A filter is a set of numerical weights
 150 that, when applied to an image, quantifies the presence of the specific shapes and/or colors that the filter is trained to detect. Figure 3 shows a selection of images which maximally activate specific filters from VGG16, with each row corresponding to one of the five convolutional blocks. Filters in earlier convolutional blocks detect simple features, such as colors, lines, corners, and blobs, while later filters detect more complex combinations of features. This aggregation of features through successive convolutional layers mirrors the process of complex feature detection in human vision. Any complex feature can be disassembled into a set of simple features; similarly, the successive sets of layers

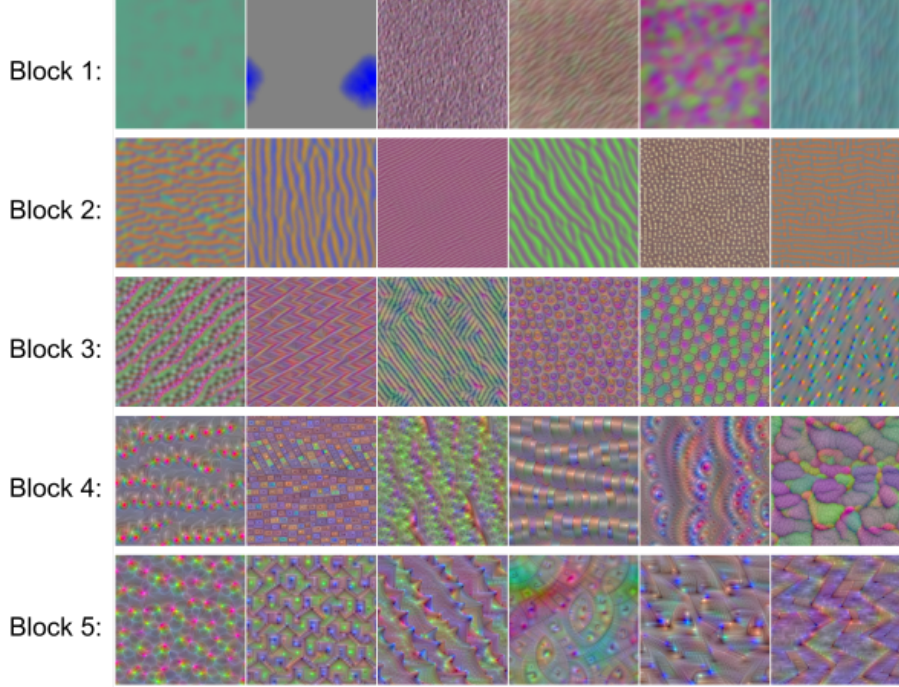


Figure 3: Visualizing convolutional filters requires generating images which maximally activate specific filters. This figure contains images that maximally activate a selection of filters from the convolutional blocks of VGG16. Filters from later blocks detect more complex features than those in earlier blocks. Much like human vision, a hierarchical structure of feature detection with increasing complexity allows CNN “vision” trained on a general task to be applied to new domains.

detect increasingly detailed features.

160 Although the filters of VGG16 have been trained and optimized on the ImageNet data, the large number of filters span a wide variety of shapes and features, many of which are useful when examining tread patterns. Just as humans can detect the features of an unfamiliar object (constituent parts, edges, textures, and corners), a CNN trained on a wide set of objects can be used to classify 165 unrelated images, such as shoe soles.

In this paper, we demonstrate the use of transfer learning to automatically identify features in shoe treads that are used by forensic examiners. To do this,

we leverage the relatively simple structure and generalizability of VGG16 and train a new classifier using a database of labeled shoe tread images we have assembled for this project. This approach differs from other approaches [10, 9, 11] in automatic footwear identification that use the output from the model base directly and do not attempt to add human-friendly contextual information with an additional classifier. The next section describes how the database of images was produced and used to fit our custom classifier.

¹⁷⁰ *Annotated Training Data.* Existing research indicates that a sufficiently well-defined set of features can be used to separate shoes into make and model categories [13]; the set of features used in that study included circle/oval, crepe, herringbone, hexagon, parallel lines, logo/lettering/numbering, perimeter lugs, star, and other. After consulting with practitioners, we developed a set of ¹⁸⁰ categories suitable for automatic recognition by convolutional neural networks. These modifications were necessary because some of the definitions used in Gross et al. (2013) require contextual spatial information which is not preserved during labeling (for example, lugs are required to be on the perimeter of the shoe). Table 1 shows three examples of each class in the modified feature set.

¹⁸⁵ The categories we use in this study are operationally defined as follows:

Bowtie Bowtie shapes are roughly quadrilateral, with two opposite concave faces. The remaining two faces can be convex or straight, and the concave faces may have straight portions, so long as there is a concave region.

¹⁹⁰ **Chevron** Chevron shapes include repeating parallel lines as well as individual “v” shapes. They may be angular but can also be curved.

Circle Circles include ellipses and ovals; they must be round.

Line Lines are repeated and parallel; a more general definition of a line would be difficult to differentiate from many other patterns. Lines can be mildly curved.

¹⁹⁵ **Polygon** Polygons are defined in this standard to have more than 4 sides. They include pentagons, hexagons, and octagons.

Quadrilateral Quadrilaterals (quads) have four sides. They may have rounded or square corners.

Star Stars are any shape with alternating concave and convex regions, or lines
200 which emanate from a central point. “X” and “+” shapes are also classified as stars.

Text Text is any shape which would be identified as text by a reasonable human. In most cases, the text on the outsole images used is made up of Latin alphabet characters; the model will likely not recognize text in other
205 scripts (but could be trained if non-Latin text images could be obtained).

Triangle Triangles are any three-sided figure. Like quadrilaterals, they can have rounded corners. In some cases, it is difficult to distinguish between a trapezoidal shape and a triangle when rounded corners are involved.

Other Other features which were marked include logos, various textures (including crepe, stippling, etc.), and smooth regions with no discernible features. These regions are grouped and provide the additional information
210 that none of the previous nine categories are present.

Thousands of outsole images were obtained from online shoe retail sites and annotated using LabelMe, a tool for image annotation in computer vision
215 problems [22]. After annotation, the minimum bounding rectangle of the region is identified and the image is cropped to that area; subsequently, the cropped image is scaled to 256 x 256 pixels. During this process, aspect ratio is not preserved, though efforts are made to label regions which are relatively square to minimize the effect of this distortion. To date, 4571 shoes have been labeled,
220 yielding 28081 multi-label images.

A reasonable critique of this approach is that images collected from online retailers are of much higher quality than would be expected from the sidewalk scanner proposed in section 1, and thus the CNN described in this paper is not immediately ready to process real degraded images. This concern is especially
225 fair when considering that machine learning methods tend to perform poorly

The figure displays a 5x10 grid of images, each showing a different 3D surface texture. The textures are categorized into five groups: Bowtie, Circle, Polygon, Star, and Triangle. Each group contains two images per row, with the exception of the 'Other' category which has one image per row.

- Bowtie:** Includes a dark grey surface with a repeating bowtie pattern and an orange surface with vertical ridges.
- Circle:** Includes an orange surface with circular indentations and a white surface with a circular indentation containing a crosshair-like pattern.
- Polygon:** Includes a teal surface with a hexagonal grid pattern and a brown surface with a larger polygonal grid pattern.
- Star:** Includes an orange surface with a four-pointed star shape and a grey surface with a multi-pointed star shape.
- Triangle:** Includes a green surface with a triangular grid pattern and a black surface with a large red triangular shape.
- Chevron:** A single yellow surface with a zigzag pattern.
- Line:** A single dark grey surface with horizontal ridges.
- Quad:** A single dark grey surface with a repeating square pattern.
- Text:** A single yellow surface with the word "titto" embossed in it.
- Other:** A single white surface with a repeating wavy pattern.

Table 1: A set of geometric elements used to classify tread patterns. Categories modified from [13].

when applied to test data that do not resemble the training data. However, the proposed automation methods for this approach are quite novel within the domain of footwear examination, and a fully functioning scanner does not yet exist to collect large amounts of degraded images. Thus, the goal of this work is to evaluate the proposed classification scheme and determine whether CNNs can sufficiently distinguish features found on outsoles. Addressing these questions with clean retailer images provides both justification for further developing the scanner and guidance for modifying the model to process real degraded images.

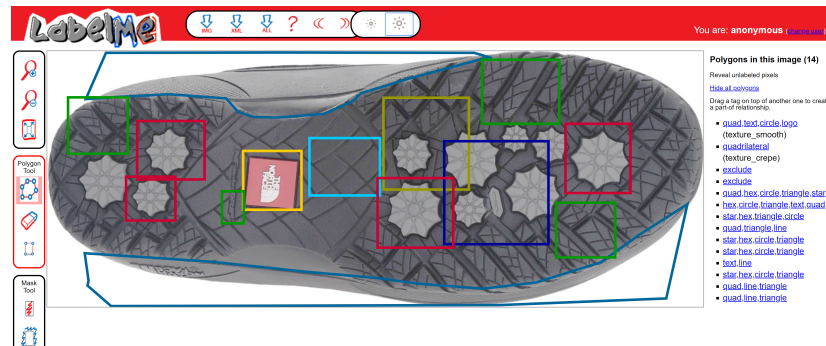


Figure 4: An example of labeling images with LabelMe

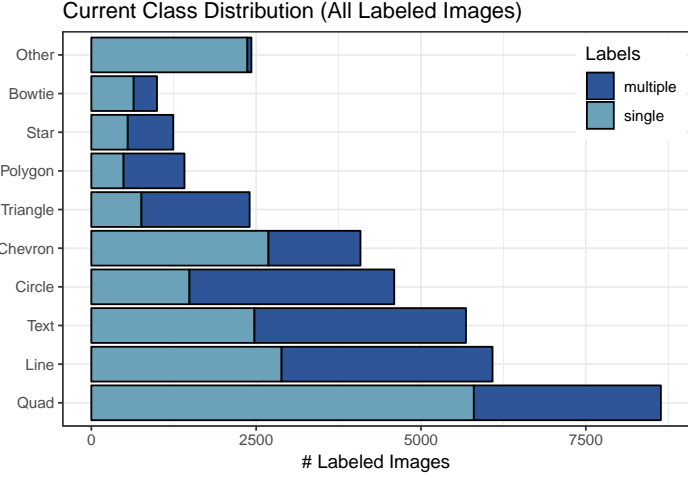


Figure 5: Distribution of classes in all labeled images. Quadrilaterals, lines, circles, text, and chevrons are relatively common; stars, polygons, and bowties are relatively rare.

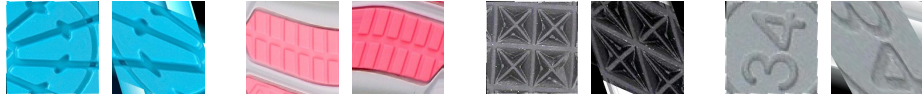


Figure 6: Four sets of original (left) and augmented (right) labeled images.

Transfer learning reduces the amount of data required to train a CNN by several orders of magnitude, but labeled images are still difficult to generate on a large scale. Thus, to make the most efficient use of the existing labeled data, we enlarge the training data using a process called image augmentation [8]. Augmentation is the transformation of original input data using image operations such as cropping, zoom, skew, rotation, and color balance modification in order to distort or alter the image while maintaining the essential features corresponding to the label. This process reduces the potential for overfitting the model to the specific set of image data used during the training process, and also increases the amount of data available for training. Examples of pre- and post-augmentation images are shown in Figure 6.

Model training is analogous to the human learning process. For example, a child learns to identify dogs by being presented with many labeled examples,

such as when their parent uses the label “dog” for an animal walking by. That child’s understanding of dogs is then measured by how many dogs the child is able to correctly identify, and also by the number of other animals it mistakenly calls “dog”. Similarly, CNN training is a series of stages, or “epochs”, where the model learns from the set of labeled training data, and that learning is measured through intermediate predictions on validation data.

The 28081 images were split such that 60% were used for training. Since the categories do not exist in equal proportion in the labeled data, the training data were weighted by proportion during the training process to ensure that the model can identify both rare and common geometric shapes. Of the remaining 40% of data, half were used for validation, to monitor the training process, and the remaining data were for testing the performance of the final model.

3. Results

260 3.1. Model Training

During model fitting, the model “learns” from the training set and is evaluated on the validation set, which consists of previously unseen images (i.e. images not used during the training process). Learning occurs by minimization of the “loss”, which is a function of the distance between the model predictions and the image labels. As the loss decreases, the model’s accuracy (the proportion of correct labels) increases. During model training, we expect that the accuracy for the training set will increase beyond the accuracy for the validation set; the validation accuracy will eventually level off. Similarly, we expect the loss for the training set and the validation set to decrease initially. Figure 7 shows the training and validation accuracy and loss at each epoch of the fitting process.

Overfitting occurs when a model learns the training data so well that its understanding of the categories becomes specific to the training cases, which, in turn, leads to poor prediction of new images that were not in the training set. During the training process, overfitting is indicated when the validation loss

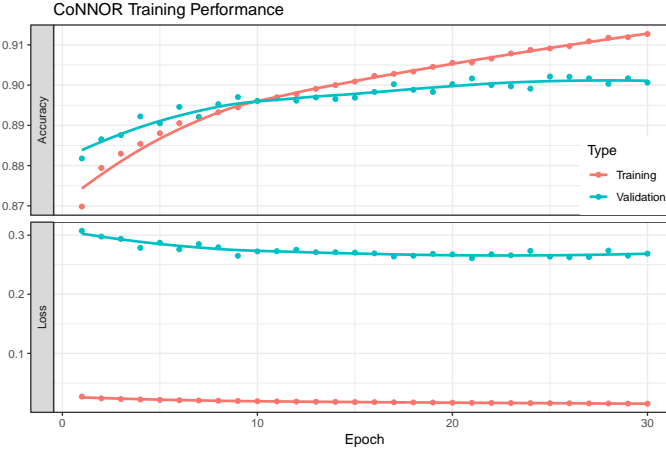


Figure 7: Training and validation accuracy and loss for each epoch of the fitting process. Training and validation accuracy reach 89.5% around epoch 9. After that point, validation loss remains the same and training loss decreases slightly, while validation accuracy increases more slowly than training accuracy.

begins to increase after reaching a global minimum. Alternately, underfitting occurs if the validation accuracy is still increasing when model optimization is terminated (for instance, between epochs 1 and 10 in Figure 7), because model performance is still improving with continued training. In Figure 7, validation accuracy levels off after epoch 20, and validation loss has not yet begun to increase at epoch 30, indicating that the model optimization process was halted at an appropriate epoch.

3.2. Model Accuracy

Overall Accuracy. For each image in the test set, the “true” labels are nine human-assigned labels of 0 or 1 corresponding to the presence or absence of each of the nine shape categories in the image. When the CNN predicts which shapes are in the image, however, it assigns a probability between 0 and 1 for each shape category, with a total of nine probabilities per test image. Thus, to determine the accuracy of the model predictions, we must select a threshold for each label to discretize the model predictions. If the threshold is too low, mod-

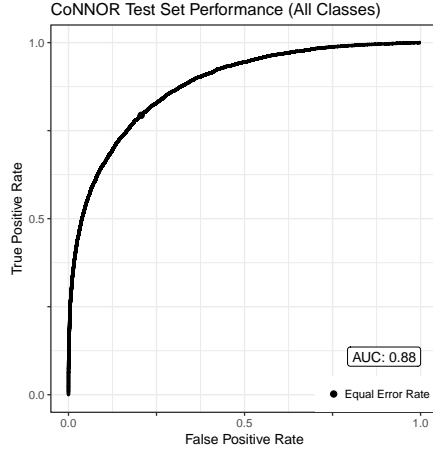


Figure 8: ROC curve showing overall model performance. Model accuracy is generally high, as the ROC curve is significantly above the identity line $y = x$.

erate probabilities will be more likely to exceed the threshold, which increases the true positive and false positive predictions in the test data. Conversely, if the threshold is too high, moderate probabilities will more often fail to meet the threshold, which increases the number of true and false negative predictions.

295 An appropriate threshold must be chosen to produce a high true positive rate while also ideally keeping the false positive rate low. One way to set an optimal threshold is to utilize Receiver Operating Characteristic (ROC) curves, a type of diagnostic plot which compare the false positive rate to the true positive rate for a classification method. Figure 8 shows the ROC curve for our model across

300 all classes, and Figure 9 shows the curve for each class. ROC curves can be summarized by the Area Under the Curve (AUC), which quantifies the overall accuracy of the model. Perfect prediction would be indicated by a right angle along the upper left corner of the plot, with a corresponding AUC of 1, and a diagonal line with an AUC of 0.5 would indicate that the classification method

305 performs no better than random chance.

The full model has an AUC of 0.88, and the AUC for individual classes ranges from 0.81 (for line) to 0.93 (for bowtie). While the class performances do vary slightly, each ROC curve indicates that the model performs significantly

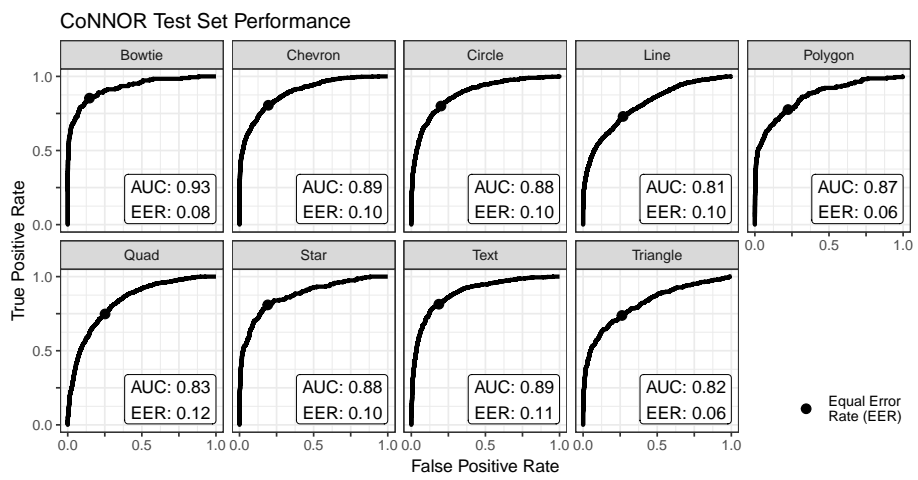


Figure 9: Class-by-class ROC curves. AUC is area under the curve, a measure of overall model performance. Equal error rates (EER) are marked, indicating the position at which there is equal probability of a false positive or false negative error.

better than random chance. The points in Figure 9 represent the equal error rate
310 (EER), which is the threshold where there is equal probability of a false positive or false negative error. We will use a class specific EER to set an individual threshold for each class, so that any model prediction with probability above the EER for that shape is considered a positive prediction.

Class Accuracy. The ROC curves provide only a general summary of model
315 accuracy; to learn more about how specific images are classified, we can view images from the test set along with the nine class predictions assigned by the model. Figure 10 and Figure 11 show model predictions for a selection of images. Each image shown in the following examples belongs to either the validation or test data, so none of the images were used during model training. In these figures, the values in each row are the predicted probabilities for the nine classes in the corresponding image, such that each column represents predictions for a given class. The saturation of blue color corresponds to the strength of the predicted probability, and the navy blue border around an image indicates that the predicted probability is above the EER threshold for the given class. Note
320 that the EER is not the same for all classes; in other words, the same probability value assigned across different categories may yield different conclusions about whether the model predicts the shape is present or absent in the image.

The first rows of Figure 10 are images which contain only one of the nine classes. Most of the predictions for these images are promising; there are
330 some false-positive labels that indicate confusions between circle/text and polygon/quad, but all of the true shapes are correctly identified by the model above their respective EER. The next image belongs to the “other” category, as it does not contain any of the nine classes; the model correctly assigns near-zero probabilities to each class. The final rows are of images that belong to more than one class category. Again, predictions are largely accurate, with most of the prominent shapes correctly identified above EER. The most notable misclassifications in these images are the false positive predictions of triangle in the image with green text and lines in the Adidas logo. Although the Adidas logo is technically
335

made up of adjacent quadrilaterals, the prediction of a triangle is reasonable
340 when considering the proximity of those quadrilaterals and the shape’s features as a whole, and the relatively low predicted probability suggests that the model recognizes that this shape is ambiguous. All other predictions for these images are accurate given our operational definition of class categories.

While figure 10 shows representative examples of classifications across multiple shape categories, it is also useful to examine many cases within a given shape to get a sense of model consistency. Figure 11 shows a number of images containing circles and/or text. The top four rows show text contained within a separate, distinct circle shape, and the next five rows show circles represented as the letter “o” in text. The remaining images contain only one of either text or circles, as well as other possible shape categories. In particular, the first two of these images contain text that use the capital letter “G”, the next two images contain no circular shapes, and the final 3 images contain pure circles that do not appear to belong to text. The model is able to identify the circle in all cases where a circle is truly present, regardless of whether the circle is part of the text or it is distinct; however, the circle prediction is also strong in three of the four images that do not contain a circle, which indicates that the model is having difficulty distinguishing the two categories. While the circle predictions are often above the EER for letters such as G and S, these predictions are generally much lower than those where distinct circles or Os are seen, indicating that there are some indications that features are not as strong in the quasi-circle shapes, but that the model is not able to completely separate Os from C, S, and G shapes which are also very circular. This confusion is complicated by the frequency of images which contain both circles and text: text is present in 39% of our labeled images containing circles, and circles are present in 31% of our images containing text. In addition, the distinction between a circle and an “o” comes from the context around the shape, which is much more difficult for the model to parse than simply detecting a shape. More importantly, this behavior does not suggest poor model performance as much as a weakness of the classification scheme, which will be discussed in a later section.

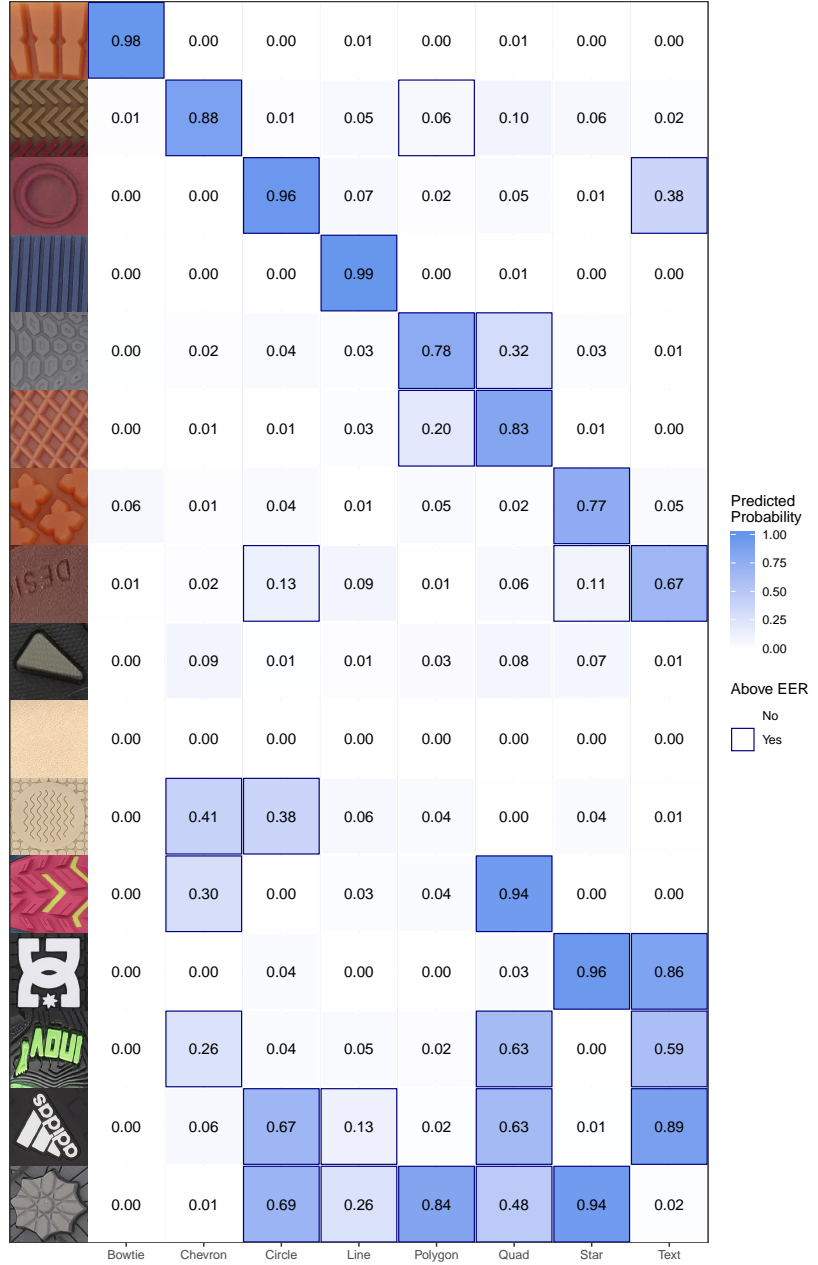


Figure 10: Model predictions of images containing (from the top) a single shape, no shape, or multiple shapes across all categories. Predicted probabilities greater than the equal error rate threshold are outlined in blue. Although there are some misclassifications, predictions are generally consistent with the human-assigned labels of these images.

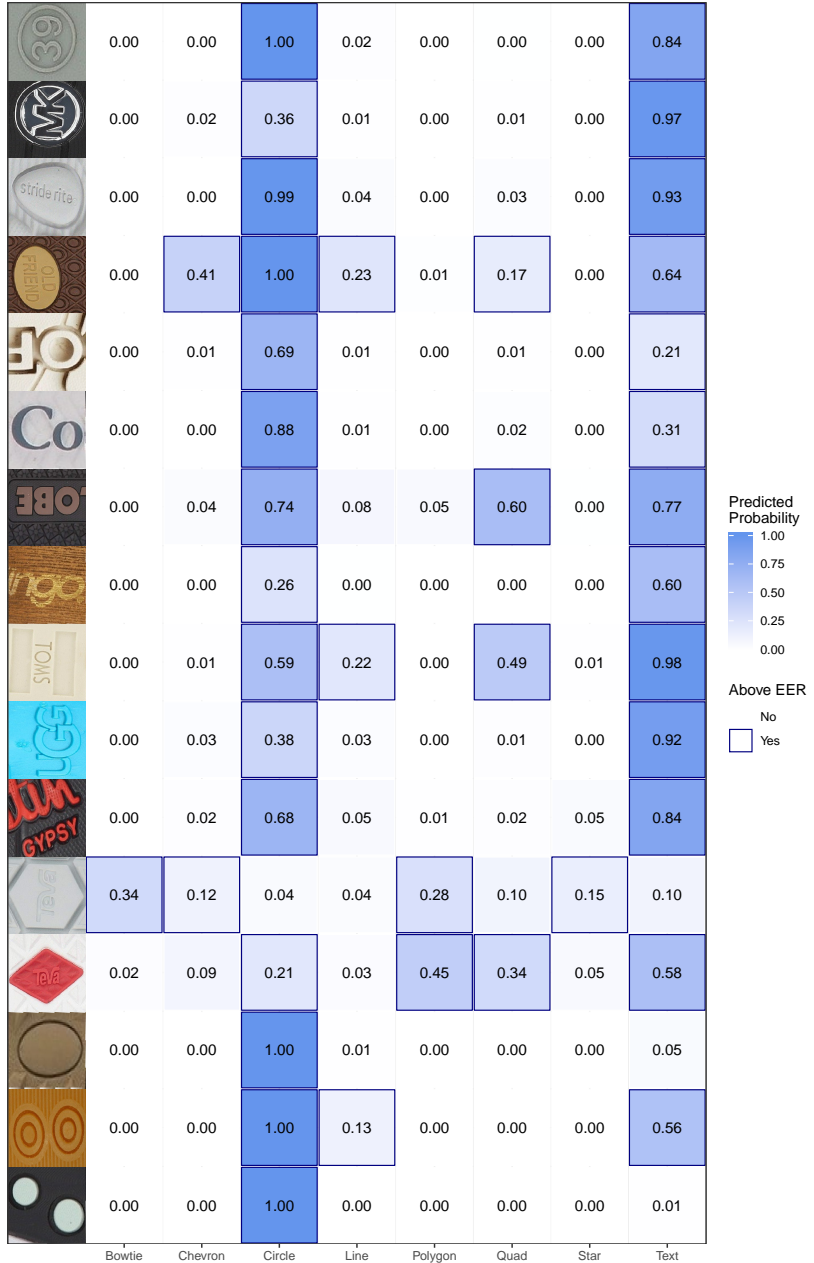


Figure 11: Model predictions of images containing circles and/or text. The model correctly identifies circles in all images where circles are present, but also predicts moderate probabilities of circles in many images where text is present with curved letters, such as “G”. Text is correctly identified in most images, with the exception of the false negative prediction of the low-contrast text within a hexagon and the false positive prediction of concentric circles.

370 Figures 10 and 11 show predictions for a number of individual images. Many
375 of the misclassifications in these examples, however, are not just seen in individual images, but rather exist systematically between certain classes. A confusion matrix is a type of visualization that summarizes the relationships between the labels assigned to an image and the labels predicted by the model across all test data, and is a helpful diagnostic tool to understand which classes are systematically misclassified. The confusion matrix for the fitted model is presented in
380 Figure 12. The values along the diagonal of the matrix represent the proportion of true positives captured within each category. The off-diagonal values represent the proportion of false positives for each shape pairing; however, since a single image may truly contain multiple shapes, the values have been adjusted to remove the effect of any true positives from the calculation of false positive proportions. Thus, this might be considered a conditional confusion matrix, because we condition the off diagonal probabilities on the label not being correct. For example, to calculate the proportion of images that contain triangles but are
385 being falsely labeled as containing quadrilaterals, any images that truly contains both triangles and quadrilaterals are removed before calculating the proportion of false quadrilateral labels. As a result of this adjustment, the off-diagonal values of the confusion matrix are the proportion of images within a true class (column-wise) that are falsely labeled as containing another class that has not
390 been labeled in the image (row-wise). Note that this matrix is not symmetric: the proportion of images containing text that are falsely predicted to contain circles is not necessarily equal to the proportion of images containing circles that are falsely predicted to contain text.

395 The horizontal band in Figure 12 indicates that quadrilaterals are predicted more often than they should be for every true label. Similarly, polygons and triangles produce a moderate number of false positive predictions in other categories, as evidenced by the vertical bands for these categories. It is also apparent that circles and text are commonly confused, which supports our earlier observations from Figure 11 that these two classes are difficult for the model to
400 distinguish, in part because circles are relatively common components of Latin

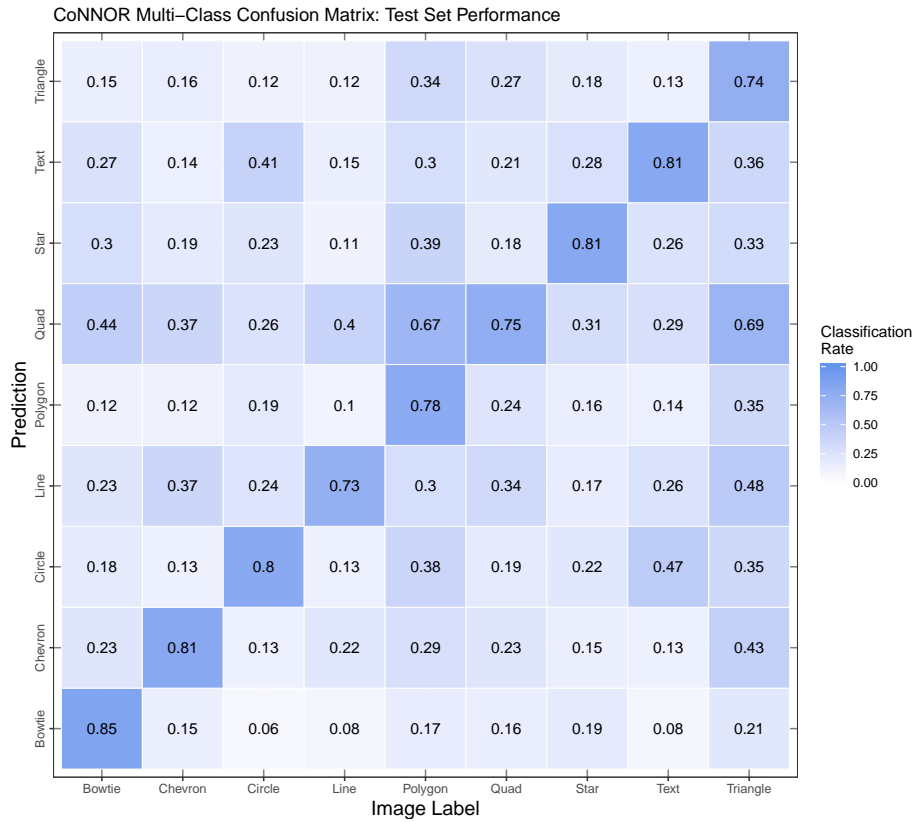


Figure 12: Confusion matrix, showing on the diagonal the correct classification rate and on the off-diagonal, classification errors. Note that in multi-label images, correct off-diagonal labels have been excluded from the calculation of false positives. Quadrilaterals are generally over-predicted across true labels; polygons and triangles are under-predicted. Circles and text are also often confused.

script characters.

3.3. Model Diagnostics

After examining model performance, both in specific cases and systematically across classes, there seem to be two primary reasons for misclassifications:
405 poor image contrast, and overlapping features between categories.

Image Contrast. As described earlier, the images used for this research were obtained from online retailers before being labeled and cropped. One consequence of using outsole images instead of impressions is the impact of colors in the image. Features from outsoles that are primarily black or white in color
410 are typically not as prominent as features from images with more varied color schemes. As a result, the features in low contrast images are not easily resolved by the filters; this is propagated through both model training and prediction of new images. In other words, the model ‘learns’ that when there are few meaningful features with which to determine which shapes are present, the best strategy
415 for minimizing loss is to predict diffuse probabilities across many classes, as seen in Figure 13.

Feature Overlap. We have defined our categories through consultation with practitioners and modifications of previous research, but as a result, there are a number of features (such as lines, angles, and curves) which are not unique to
420 only one category. For example:

- a triangle may be made up of three acute angles, but a quadrilateral can also contain three acute angles.
- the only distinction between an “o” and a circle is whether there is more text around it.
- 425 • the only difference between lines and thin repeating quads are the ends of the shapes.

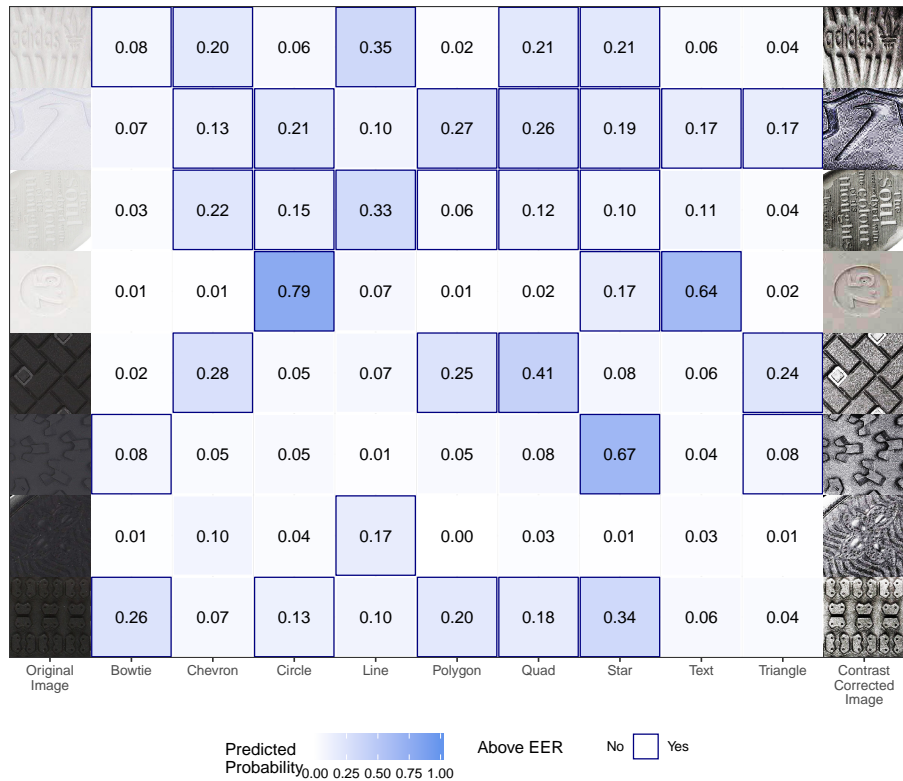


Figure 13: Model predictions for images with low contrast. While these images contain a variety of shapes (as shown in the color-corrected column on the right), the diffuse probabilities assigned by the model across all categories indicate that features are obscured by low contrast, which propagates through model training and prediction.

To detect these shapes, the model is doing a significant amount of feature integration beyond just detecting the presence of raw lines, angles, and curves. A correct classification requires the detection and integration of (often) relatively large features (with respect to filters only a few pixels wide); in addition, features can be relatively small relative to the 256x256 image, or may take up the entire image. This wide variation in relative size of the features, combined with the variability of different features across classes, leads to a number of common (but understandable) misclassifications.

This is one area where the CNN's predictions do not match human labels; in part, this is because even with some wider context, the CNN does not use both bottom-up feature integration and top-down object identification based on wider experience - as a result, it cannot easily differentiate between text and constituent shapes within the text.

This issue is exacerbated by the variability of images within a class. A quadrilateral isn't just a square or rectangle with 4 right angles; it can also be a parallelogram, diamond, trapezoid, part of a chevron, or anything else that has four sides. In general, some of our identified shapes are very common on outsoles and appear in our data in many different forms, which further widens the sets of features the model must learn to associate with a single class. Unfortunately, by associating even more possible features with a single category, the number of features that then overlap between categories also increases.

The shape categories with the largest number of images, shown in Figure 5, also tend to have the most variability in labeled images. This is supported by Figure 14, which breaks down, by proportion, the top ten most frequent brands in the labeled data for each class. The figure shows that, for example, a relatively large proportion of bowties in our labeled data are contributed by images of Birkenstocks. Since the bowties on Birkenstocks tend to be similar in shape and size, the model is able to create a relatively stable definition of bowties and thus predicts new images of bowties well. There is no similar consistency in categories like quadrilaterals. Figure 14 indicates that no one brand makes up more than 4% of our labeled quadrilateral images. This suggests that the

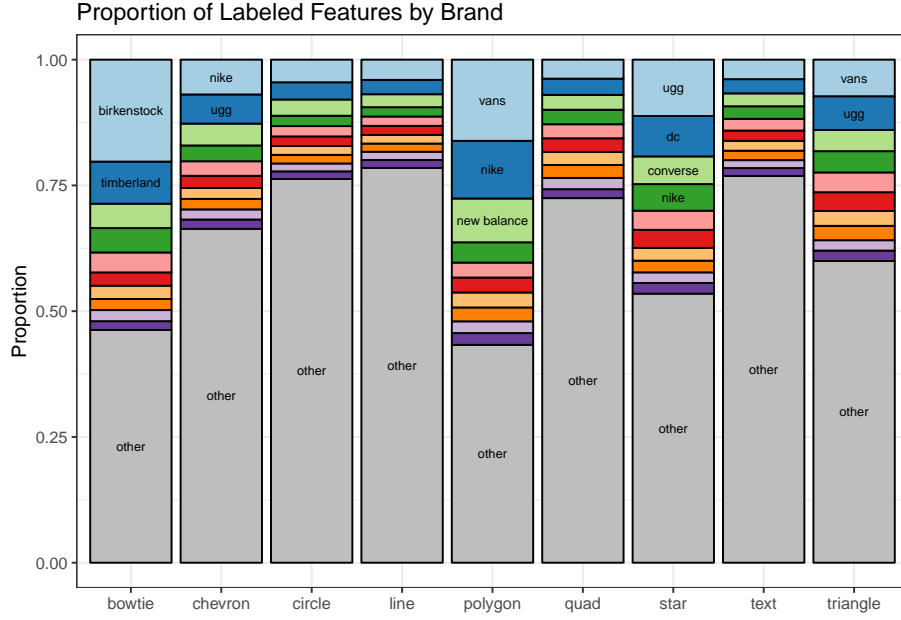


Figure 14: Proportions of top 10 shoe brands in our labeled dataset within each shape category, sorted by prevalence. Brand text is present when the brand makes up more than five percent of labeled shoes for the shape category. Some shapes, like bowtie and polygon, are relatively dominated by a small number of brands while other shapes, such as text and quad, are comprised of a large number of brands. Typically, model predictions are best for shape categories without much variability, which, in general, coincides with shapes dominated by a small number of brands.

quadrilaterals in our labeled data are more likely to come in a variety of shapes and sizes, so it is more difficult for the model to learn which set or sets of features correspond to a quadrilateral.
460

We have proposed several hypotheses to explain the inconsistencies between the manual labels and the model’s predictions on the images. We can test these hypotheses by examining what the model “sees” when making its predictions. Heatmaps, also known as Class Activation Maps (CAMs), are a visual diagnostic tool that highlights the areas of an image that are most significant to classification for a given class [23]. Using these graphics, we can identify which locations in an image contribute most to the model’s predictions.
465

Figures 15-17 show a number of images alongside heatmaps for the four classes with the highest output probabilities for each image. Figure 15 shows predictions and heatmaps for the logo from an UGG shoe. The model correctly identifies triangles and text, and references appropriate regions of the image. The prediction of a circle is shown to be associated with the letter “G”; although this prediction is technically incorrect, it indicates that the model has learned to associate curved shapes with circles. This association is again seen in the high predicted probability of circle in Figure 16. In this case, the prediction of text is again correct,, but the prediction of circle is not—there are very round shapes, but they do not form a closed figure that could be identified as a circle. Figure 17 shows a DC shoe with repeating instances of a shape that is a combination of a circle and quadrilateral, but does not technically fall into either of those categories by our definition. The model assigns high probabilities of circle and quadrilateral and indicates that the proper image features are being used for this classification. Additionally, the prediction of polygon is incorrect but reasonable considering that many small hexagons are indistinguishable from circles. These heatmaps can confirm that a number of misclassifications are a result of overlapping features between classes, and that the model is using reasonable features to make predictions.

4. Conclusions

The goal of this research was to develop a method to automatically identify geometric class characteristics of shoe outsoles. This goal is motivated by the desire to compute the random match probability of specific tread patterns, which could be achieved by applying this automatic image processing method to outsole images collected from a footwear scanner in a local population.

A set of geometric class characteristics was defined, based on feature sets currently used by examiners, to both broadly classify a large variety of shoes and to narrow down similarity into a manageable number and type of features for further use in a shoeprint analysis. Thousands of outsole images were obtained

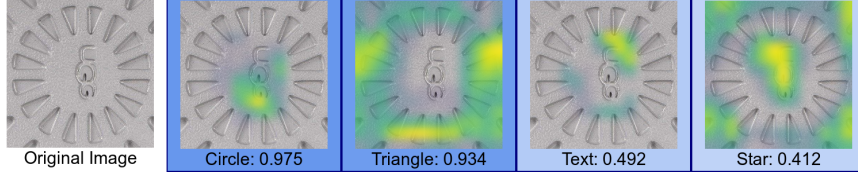


Figure 15: A section of an UGG shoe containing the logo. The model correctly identifies triangles and text (and references the correct portion of the image in both cases). The model identifies a circle as well; while it could be argued that the triangles form an implicit circle, the heatmap demonstrates that the circular portion of the image is the “G”, which would not be a closed figure labeled as a circle. The model’s prediction of the presence of a circle is understandable, but incorrect.



Figure 16: In this image of a Seychelles shoe, the model identifies text and circle. The prediction of text is correct; the prediction of circle is not—there are very round shapes, but they do not form a closed figure that could be identified as a circle.



Figure 17: This image from a DC shoe contains repeating instances of a shape that appears to be a combination of a circle and quadrilateral, but does not technically fall into any of the nine categories used in our labeling scheme. The model assigns high probabilities of circle and quadrilateral and indicates that the proper image features are being used for this classification. The prediction of polygon is incorrect but reasonable considering that many small hexagons are indistinguishable from circles.

from online shoe retailers and labeled according to their geometric shapes. The pre-trained convolutional base of VGG16 was then used, with a new classifier trained on a portion of these labeled images, to output predicted probabilities
500 for test images within the defined set of geometric features. After training, the model performs well on the data provided. In general, the model is able to identify many well-defined geometric shapes in the images.

Although model predictions are generally accurate, there are a number of systematic misclassifications. The model has substantial difficulty predicting
505 images with low contrast because image features are obscured. Exploring methods of color correction, such as histogram equalization, may prove useful for eliminating the effect of contrast on predictions. Initial implementations of histogram equalization suggest that the overall accuracy improvement is modest; the model fit to images which have been equalized had approximately 92.5%
510 validation accuracy, an improvement of 1.5% over the default model described in this paper.

Another source of systematic misclassifications stems from the inherent overlap between features of common geometric shapes. CNNs make predictions via bottom-up feature integration; as a result, it is more difficult for the model to
515 distinguish between geometrically similar shapes, such as chevrons and triangles. This issue is exacerbated by high variability of some shapes commonly found in outsole patterns, which requires the model to form a flexible understanding of each shape category and makes distinction between similar shapes even more difficult. These issues of overlap and variability are at least in part due to our
520 decision to use the features used by practitioners directly; some of this may also result from our operational definitions of various shapes, which were created before we had a complete understanding of the practical limitations of CNNs. While a complete remedy may not be possible, there may be some modifications to operational class definitions that we can make to optimize labels for model
525 prediction. In addition, we will continue to improve the labeling of shapes in our database with the goal of expanding the breadth and quantity of labeled images available for model training.

Although there are many areas for potential improvement in future iterations of this model, we have demonstrated the effectiveness of using transfer learning to provide an initial label for shoe outsole patterns. As most of the misclassifications are systematic, it is clear that the model is able to learn features and apply rules consistently. We expect that the proposed modifications to the labeling criteria and data processing pipeline will improve the model's accuracy, but the 91% validation accuracy is promising considering that we do not have estimates of the consistency of examiners' estimates on ambiguous features. Taken together, these factors show that Convolutional Neural Networks are a useful tool for classifying a large number of outsoles within a common classification scheme, although further research is needed into designing human comprehensible and yet useful classification schemes for this purpose. This work thus provides promising evidence that a well-trained model within an appropriate classification scheme, in conjunction with images collected from a footwear scanner, can be used to estimate the random match probability of footwear tread patterns.

References

- [1] M. B. Smith, The forensic analysis of footwear impression evidence (Mar 2011).
URL https://archives.fbi.gov/archives/about-us/lab/forensic-science-communications/fsc/july2009/review/2009_07_review02.htm
- [2] Parent, Sandy, Significance of Class association of Shoe Prints, 00000.
URL <https://www.slideserve.com/ayasha/significance-of-class-association-of-shoe-prints>
- [3] I. Benedict, E. Corke, R. Morgan-Smith, P. Maynard, J. M. Curran, J. Buckleton, C. Roux, Geographical variation of shoeprint comparison class correspondences, Science and Justice 54 (5) (2014) 335–337, 00001.

- [4] A. Alexander, A. Bouridane, D. Crookes, Automatic classification and recognition of shoeprints, in: *Image Processing And Its Applications*, 1999. Seventh International Conference on (Conf. Publ. No. 465), Vol. 2, 1999, pp. 638–641 vol.2. doi:10.1049/cp:19990401.
- 560 [5] M. Pavlou, N. M. Allinson, Automatic extraction and classification of footwear patterns, in: *International Conference on Intelligent Data Engineering and Automated Learning*, Springer, 2006, pp. 721–728.
- 565 [6] M. Gueham, A. Bouridane, D. Crookes, O. Nibouche, Automatic Recognition of Shoeprints using Fourier-Mellin Transform, in: *2008 NASA/ESA Conference on Adaptive Hardware and Systems*, 2008, pp. 487–491. doi:10.1109/AHS.2008.48.
- 570 [7] T. Luostarinen, A. Lehmussola, Measuring the Accuracy of Automatic Shoeprint Recognition Methods, *Journal of Forensic Sciences* 59 (6) (2014) 1627–1634. doi:10.1111/1556-4029.12474.
URL <http://doi.wiley.com/10.1111/1556-4029.12474>
- 575 [8] A. Krizhevsky, I. Sutskever, G. E. Hinton, ImageNet Classification with Deep Convolutional Neural Networks, in: F. Pereira, C. J. C. Burges, L. Bottou, K. Q. Weinberger (Eds.), *Advances in Neural Information Processing Systems* 25, Curran Associates, Inc., 2012, pp. 1097–1105.
- 580 [9] B. Kong, J. Supancic, D. Ramanan, C. C. Fowlkes, Cross-Domain Image Matching with Deep Feature Maps, *International Journal of Computer Vision* doi:10.1007/s11263-018-01143-3.
URL <http://arxiv.org/abs/1804.02367>
- [10] B. Kong, J. Supancic, D. Ramanan, C. Fowlkes, Cross-Domain Forensic Shoeprint Matching, *British Machine Vision Conference* (2017) 17.
- 580 [11] Y. Zhang, H. Fu, E. Dellandréa, L. Chen, Adapting Convolutional Neural Networks on the Shoeprint Retrieval for Forensic Use, in: J. Zhou, Y. Wang, Z. Sun, Y. Xu, L. Shen, J. Feng, S. Shan, Y. Qiao, Z. Guo,

585 S. Yu (Eds.), Biometric Recognition, Lecture Notes in Computer Science,
Springer International Publishing, 2017, pp. 520–527.

- [12] R. J. Davis, An Intelligence Approach to Footwear Marks and Toolmarks, Journal of the Forensic Science Society 21 (3) (1981) 183–193.
- [13] S. Gross, D. Jeppesen, C. Neumann, The variability and significance of class characteristics in footwear impressions, Journal of Forensic Identification 63 (3) (2013) 332.
- [14] D. Ballard, Generalizing the Hough transform to detect arbitrary shapes, Pattern Recognition 13 (2) (1981) 111–122.
doi:10.1016/0031-3203(81)90009-1.
URL <http://linkinghub.elsevier.com/retrieve/pii/0031320381900091>
- 595 [15] R. Jain, R. Kasturi, B. G. Schunck, Machine vision, 1st Edition, McGraw-Hill Science/Engineering/Math, 1995.
URL <http://gen.lib.rus.ec/book/index.php?md5=96A703D27596EB72EE3A6521525EF9CC>
- 600 [16] M. Oquab, L. Bottou, I. Laptev, J. Sivic, Learning and Transferring Mid-level Image Representations Using Convolutional Neural Networks, in: 2014 IEEE Conference on Computer Vision and Pattern Recognition, IEEE, Columbus, OH, USA, 2014, pp. 1717–1724. doi:10.1109/CVPR.2014.222.
URL <http://ieeexplore.ieee.org/lpdocs/epic03/wrapper.htm?arnumber=6909618>
- [17] J. Yosinski, J. Clune, Y. Bengio, H. Lipson, How transferable are features in deep neural networks?, in: Z. Ghahramani, M. Welling, C. Cortes, N. D. Lawrence, K. Q. Weinberger (Eds.), Advances in Neural Information Processing Systems 27, Curran Associates, Inc., 2014, pp. 3320–3328.
610 URL <http://papers.nips.cc/paper/5347-how-transferable-are-features-in-deep-neural-networks.pdf>

- [18] H. Shin, H. R. Roth, M. Gao, L. Lu, Z. Xu, I. Nogues, J. Yao, D. Mollura, R. M. Summers, Deep Convolutional Neural Networks for Computer-Aided Detection: CNN Architectures, Dataset Characteristics and Transfer Learning, *IEEE Transactions on Medical Imaging* 35 (5) (2016) 1285–1298.
615
doi:10.1109/TMI.2016.2528162.
- [19] J. Deng, W. Dong, R. Socher, L.-J. Li, K. Li, L. Fei-Fei, ImageNet: A Large-Scale Hierarchical Image Database 8.
- [20] Z. Zhong, L. Jin, S. Zhang, Z. Feng, DeepText: A Unified Framework for Text Proposal Generation and Text Detection in Natural Images, arXiv:1605.07314 [cs].
620
URL <http://arxiv.org/abs/1605.07314>
- [21] B. Liu, X. Zhang, Z. Gao, L. Chen, Weld Defect Images Classification with VGG16-Based Neural Network, in: G. Zhai, J. Zhou, X. Yang (Eds.), Digital TV and Wireless Multimedia Communication, Communications in Computer and Information Science, Springer Singapore, 2018, pp. 215–223.
625
- [22] B. C. Russell, A. Torralba, K. P. Murphy, W. T. Freeman, LabelMe: A Database and Web-Based Tool for Image Annotation, *International Journal of Computer Vision* 77 (1-3) (2008) 157–173. doi:10.1007/s11263-007-0090-8.
630
URL <http://link.springer.com/10.1007/s11263-007-0090-8>
- [23] F. Chollet, J. Allaire, Deep Learning with R, Manning Publications Company, 2018.